Condensed title: *B. leachii* whole-body regeneration

Manuscript title:

Hematological analysis of the ascidian *Botrylloides leachii* (Savigny, 1816) during whole-body regeneration

Simon Blanchoud[1,a], Lisa Zondag[1], Miles D. Lamare[2] and Megan J. Wilson[1]*

[1]Department of Anatomy, Otago School of Medical Sciences; [2]Department of Marine Science, Division of Sciences; [1,2]University of Otago, P.O. Box 56, Dunedin 9054, New Zealand.

*corresponding author: Ph. +64 3 4704695, Fax: +64 479 7254, meganj.wilson@otago.ac.nz

Abbreviations: filtered seawater (FSW), particle image velocimetry (PIV), whole-body regeneration (WBR)

Keywords: *Botrylloides leachii*, hemocytes, hemolymph flow, histology, whole-body regeneration

Highlights:

- Time-lapse recordings of hemolymph circulation
- Generalized classification system for *Botrylloides leachii* hemocytes
- Detailed analysis of regenerating and asexual budding by histology
- Synchronized contractions of ampullae following zooid removal

DOI: 10.1086/692841

Graphical TOC:

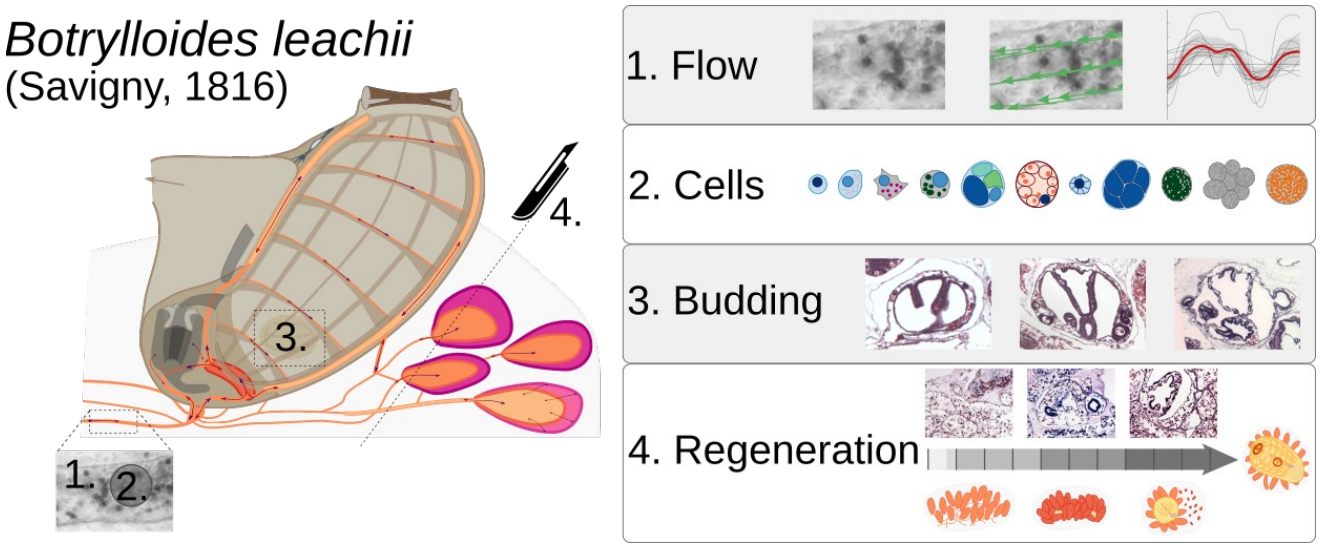

a) Present address: Department of Biology, University of Fribourg, Chemin du Musée 10, 1700 Fribourg, Switzerland.

Abstract

Whole-body regeneration, the formation of an entire adult from only a small fragment of its own tissue, is extremely rare among chordates. Exceptionally, in the colonial ascidian *Botrylloides leachii*, a fully functional adult is formed from their common vascular system, upon ablation of all adults from the colony, in just 10 days thanks to their high blastogenetic potential. While previous studies have identified key genetic markers and morphological changes, no study has yet focused on the hematological aspects of regeneration despite the major involvement of the remaining vascular system and the contained hemocytes in this process. To dissect this process, we analyzed colony blood flow patterns using time-lapse microscopy to obtain a quantitative description of the velocity, reversal pattern, and average distance travelled by hemocytes. We also observed that flows present during regeneration are powered by temporally and spatially synchronized contractions of the terminal ampullae. In addition, we revised previous studies on *B. leachii* hematology as well as asexual development using histological sectioning, and compared the role of hemocytes during whole-body regeneration. We found that regeneration starts with a rapid healing response characterized by hemocyte aggregation and infiltration of immunocytes, followed by increased activity of hemoblasts, recruitment of macrophage-like cells for clearing the tissues of debris, and their subsequent disappearance from the circulation concomitant with the maturation of a single regenerated adult. Overall, we provide a uniquely detailed account of the hematological properties of regenerating *B. leachii* colonies, providing novel lines of inquiry towards the decipherment of regeneration in chordates.

Introduction

Whole-body regeneration (WBR) is the process whereby an entire functional adult is formed from only a minute fragment of the original organism. Multicellular animals capable of varying degrees of regeneration are distributed widely throughout the metazoa , thus suggesting that this biological phenomenon has a primordial origin. However, this regeneration ability correlates inversely with body and tissue complexity .

Among vertebrates, while most adults heal only through scarring, teleost fish and urodele amphibians can regenerate tissues, body parts or organs following injury . Although the study of these organisms has brought an extensive knowledge on patterning and cellular programs required for regeneration in mature animals following severe injury, no vertebrate has yet been shown to undergo WBR. Therefore, deciphering the mechanisms underlying regeneration in evolutionarily related organisms might provide new implications about the basic principles of cellular plasticity in adult organisms of our phylum.

Tunicates represent the closest phylogenetic relative of vertebrates . In particular, colonial ascidians can undergo WBR due to their high blastogenetic potential . Belonging to the phylum Chordata, class Ascidiacea, these invertebrates have tissue and organ complexity incipient to that of vertebrates (see Fig. 1), including a well-developed notochord, dorsal nerve cord, and a post-anal tail during their free-living tadpole larval stage. In particular, *Botrylloides leachii* (order Stolidobranchia, family Styelidae; can undergo WBR in as few as 10 days . Consequently, *B. leachii* has recently emerged as a model organism for the study of regeneration .

B. leachii is a sessile suspension-feeding ascidian that live in clonal colonies of adults, termed zooids, which organize in a series of ladder-like parallel rows, known as systems (Fig. 1 A-B; . The colony attaches to its substrate, typically on seagrass or underneath rocks in the shallow sub-tidal zone, through a gelatinous tunic. While each zooid has an independent heart and an open hemocoelic circulatory system, the entire colony shares a common vascular system that is embedded in the tunic and closed at its periphery by terminal ampullae, the contractile blind ends of marginal vessels (Fig. 1 C-F; . *B. leachii* zooids are hermaphrodites and can reproduce both sexually, to colonize new locations through a tadpole larval stage, or asexually, to expand the colony . This latter reproduction, also known as palleal budding or blastogenesis , occurs on the outer epithelial mantle of a zooid, typically on both of its sides thus producing two offspring. These growing buds start as a thickened disk of cells on the body wall, protrude outwards and invaginate their inner layer to form the required layers of tissue for organ development. Eventually, these buds, located on either side of the older zooid, will mature into new adults while their parent will be resorbed by the colony . As in the closely related genus *Botryllus* , bud development is synchronous throughout the colony and starts very early in the life cycle of the parent bud .

In addition to these two methods of reproduction, *B. leachii* colonies can undergo WBR from a minute fragment of their vascular tissue (~200 cells; . WBR will only be triggered following the loss of all zooids from the colony; otherwise a more traditional injury healing will occur . *B. leachii* WBR has been reported to start with the healing of the injury sites to prevent further hemolymph loss, followed by the compaction of the marginal ampullae towards the centre of the remaining matrix. Within this reorganized tissue, regeneration niches – a discrete regeneration locus within the vascular system – will develop and apparently compete through a yet undetermined process that ultimately leads to the development of a single adult zooid, while all other niches are absorbed by the colony (Fig. 1 G). Importantly, WBR ability in *B. leachii* is retained throughout its developmental cycle , in contrast to the sister species *Botryllus schlosseri*, where WBR potential is only present during a one-day period of their asexual reproduction cycle, known as takeover . While the exact origin of the totipotent stem-like cells responsible for WBR remains unknown, it has been reported that even though they will develop a regeneration niche within the vascular system, they are not part of the circulating blood cells (hemocytes) in uninjured colonies but rather appear to migrate from the vascular lining into the vascular system after injury (.

Similar to most other chordates, ascidian hemocytes are continually renewed to compensate for cell death and external sources of loss . The location of hemopoiesis in ascidians is still debated, which might be a consequence of the variety of developmental strategies observed among this clade . In some solitary ascidians, it principally occurs in small static clusters of hemoblasts located in the lining of the hemocoel, particularly around the pharyngeal basket . In colonial ascidians, clusters of undifferentiated cells with pluripotent properties, called islands, have been detected in the sub-endostylar ventral sinus . In addition, ventral islands located near the endostyle have been identified as sites of phagocyte turnover . Furthermore, circulating hemoblasts have been shown to express stemness and proliferation markers around early buds of *Botrylloides violaceus*, suggesting a circulatory source of hemocytes . It thus appears that there may be multiple sites for ascidian blood (hemolymph) production, in particular in colonial tunicates. Hemolymph is mostly colorless and composed of a variety of cell types with functions incipient to that of vertebrates ; and its flow patterns are intimately linked to the health of the whole colony .

Although there has been a number of studies investigating the morphotypes of ascidian hemocytes , including of *B. leachii*'s , improved resolution and color images would benefit future work on this species. In addition, no common terminology has been accepted to identify these cell types, mainly because of discrepancies between their phenotype and their function in different species, as well as a lack of understanding of their differentiation lineages . Furthermore, accurate identification is crucial for detecting and interpreting variations in the sub-populations of hemocytes during WBR.

Despite the major involvement of the remaining vascular system and the comprised hemocytes during WBR in *B. leachii*, no study has yet focused on the hematological aspects of regeneration. To obtain a more accurate understanding of the WBR process in *B. leachii*, we set out to characterize, in a consistent and amended approach, both uninjured and regenerating colonies at the circulatory, tissue, and cellular levels. We used both histological staining and time-lapse recording to dissect this highly dynamic process of regeneration with greater resolution.

Experimental procedures

Animal husbandry and manipulation

B. leachii colonies were collected from the two sites in the Otago Harbor (45°52'12"S, 170°31'48"E and 45°49'41"S, 170°38'29"E), and Nelson Harbor (41°15'36"S, 173°16'48"E), New Zealand between September and March over 2014 to 2016. *B. leachii* grows naturally on submerged structures (e.g. ropes, pontoons, tires), and colonies were removed from the attached substrata with a single edge razor blade. Each colony was placed on either 5.0×7.5-cm or 2.6×7.6-cm glass slides and left horizontally for two days in 200 ml of still seawater, changed daily, to allow the colony to attach to the slide. The slides were then placed vertically and kept at the Portobello Marine Laboratory (University of Otago) in a tank supplied with a constant flow-through of filtered seawater directly from the harbor, with temperature controlled between 18 °C and 20 °C. The glass slides were kept clear of algal growth by using a paintbrush and a single edge razor blade . Colonies were continuously fed, using a peristaltic pump, a 1:1:1:1 by volume mixture of three algae (*Chaetoceros muelleri*, *Pavlova lutheri* and *Tetraselmis chuii*) and a rotifer (*Brachionus plicatilis*) culture, complemented with Alltech All-G-Rich algae/yeast powder mix (12 g of Alltech All-G-Rich were added each week to the rotifer culture).

B. leachii hemolymph was collected as previously described . Briefly, whole colonies were first cleaned using filtered seawater (FSW) and incubated for 5 min in anticoagulant solution (0.38 g sodium citrate per 100 ml FSW, pH 7.5). To prevent loss of hemocytes, all instruments were incubated twice for 1 min in the anticoagulant solution prior to collection. Colonies were then dried using blotting paper and their marginal vessels broken using a needle. The hemolymph was then collected using a syringe and transferred into a 1.5-ml microfuge tube containing 100 µl of the anticoagulant solution up to a total volume of 600 µl. The tube was left 5 min on ice and the supernatant transferred to a new tube to remove debris. Following centrifugation at 780 g for 12 min, the supernatant was discarded and the pellet re-suspended in 100 µl FSW.

B. leachii regeneration was carried out following an established protocol . Dissection of adults and buds away from the marginal ampullae, during their mid-cycle blastogenic stage (i.e. not undergoing take-over), was carried out using a scalpel and a single edge razor blade. The slides with the remaining vascular fragments were then placed into an aerated seawater tank at 19 °C and left to regenerate until a certain morphological stage had been reached.

Histological staining

B. leachii regenerating tissue fragments were fixed overnight in 4% para-formaldehyde (PFA) in FSW, dehydrated in 70 % ethanol (EtOH) and embedded in paraffin wax. The fragments were then sectioned (5 µm thickness*)* in the transverse plane. Three stains were used on dewaxed slides: hematoxylin and eosin (H&E), Giemsa, and Martius Scarlet Blue trichrome (MSB). H&E staining was performed as follows: stain for 4 min in hematoxylin (Leica Biosystems Surgipath Gill II hematoxylin), wash for 2 min in running tap water, place the slide for 2 min in Scott's tap water (2 g of potassium bicarbonate, 20 g magnesium sulphate per liter), wash again for 2 min, stain for 30 s in eosin (Leica Biosystems Surgipath Eosin), wash for 1 min, dehydrate and mount. Giemsa staining was performed as follows: stain for 30 min in a coplin jar containing Giemsa (7.36 g Giemsa powder in 500 ml of 50 °C glycerol and 500 ml methanol, mix 1:45 in dH_2O) within a 56 °C water-bath, rinse in dH_2O, differentiate in 1/1500 acetic acid solution, rinse in dH_2O, dehydrate and mount. MSB staining was performed as follows: stain for 5 min in Celestine blue (5 g ferric ammonium sulphate, 0.5 g Celestine Blue B in 100 ml dH_2O with 14 ml glycerol), wash for 30 s in running tap water, stain for 5 min in hematoxylin, wash again for 2 min, place the slide for 2 min in Scott's tap water, wash for 2min, rinse for 1min in 95 % ethanol, stain for 2 min in Martius yellow (20 g phosphotungstic acid, 5 g martius yellow per liter of 95 % ethanol), rinse three times for 1 min in dH_2O, stain for 10 min in brilliant scarlet (10 g brilliant scarlet crystal ponceau 6R, 20 ml glacial acetic acid per liter of dH_2O), rinse again three times, place the slide for 4 min in phosphotungstic acid (10 g per liter of dH_2O), rinse for 1 min in dH_2O, stain for 45 s in methyl blue (5 g methyl blue, 10 ml glacial acetic acid per liter of dH_2O), rinse for 1 min in acetic acid (10 ml glacial acetic acid per liter of dH_2O), dehydrate and mount.

Hemolymph smears were obtained as previously described . Briefly, drops of 50 µl of isolated hemocytes (see above) were left for 30 min to attach on SuperFrost Plus (Thermo Fisher Scientific) microscopy slides. The drop was then discarded by placing the slide vertically and the remaining attached cells were fixed for 30 min at 4 °C in ascidian fixative solution (1 g NaCl and 1 g sucrose in 1 % glutaraldehyde in FSW). Slides were then rinsed for 10 min in 0.1 M PBS, stained using 10 % Giemsa, mounted using a 9:1 glycerol-PBS solution and sealed with a coverslip using nail polish.

Imaging

All fixed samples were imaged on an Olympus AX70 microscope equipped with a QImaging MicroPublisher 5.0 2560×1920 pixels camera using QCapture. Magnification used ranged from 4 x to 100 x. Time-lapse recordings of hemolymph flow in live colonies were acquired on a Leica M205 FA stereo-microscope equipped with an 8 megapixel CCD DFC490 color camera using the Leica Application Suite (LAS). Recordings were acquired using the "Movie" continuous mode, at different magnifications (7.42 x to 20 x) and exposure times (27.7 ms to 55.7 ms) adapted to the recorded portions of the colony, with a resolution of either 544×408 or 1088×816 pixels.

Data processing

Acquired images were processed for color balance using the open-source Gimp program (The GIMP development team) and assembled into figures using the open-source Inkscape software (The Inkscape Project). Colors were chosen according to the ColorBrewer palette (Cynthia A. Brewer, Penn State). Movies were montaged using the Lightworks program (EditShare) and compressed using the open-source HandBreak tool (The Handbreak Team).

Hemolymph composition during WBR was estimated by manually identifying cell types in microscopy images using five randomly located images of Giemsa stained ampullae, at a 60-x magnification. Similarly, 10 images were used to characterize hemolymph composition in intact colonies fixed during their mid-cycle blastogenic stage. Only cells located inside the ampullae, centered on the imaged section and unambiguously identified (2.6 % of the total 2339 cells could not be determined) were considered. Between 272 and 447 cells were positively identified for each stage of regeneration, 502 for the intact colony. We focused our counting on ampullae for setting up a meaningful comparison between intact and regenerating tissues as blood vessels become very sparse after tissue contraction.

The appearance of hemocytes was characterized using light microscopy by smearing ascidian hemolymph and by staining histological sections of whole colonies.

Computational analysis

Vessel identification in time-lapse recordings was performed as follows. Raw frames of the recording were smoothed using a Gaussian kernel of radius 0.89 µm, the difference between consecutive frames was computed and moving cells were identified as having an absolute value greater than 6 x the estimated standard deviation of the image's white noise (. Cells larger than 5 μm^2 were then consecutively morphologically dilated and eroded, using structuring disks of radii 41 µm and 21 µm, respectively. The resulting detections were then averaged over the entire recording, and vessels defined as containing moving cells in at least 30 % of the frames. The location, length and width the vascular systems were then identified using the morphological skeleton of the vessels.

Hemolymph flow was measured using a particle image velocimetry (PIV) approach with multiple passes and sub-pixel resolution using Fourier-space based on the difference between consecutive frames. Raw frames of the recording were smoothed using a Gaussian kernel of radius 0.89 µm, the difference between consecutive frames was computed and PIV performed between two consecutive differences, using a modified version of `matpiv_nfft` from the MatPIV toolbox (Johan K. Sveen, University of Oslo), through four consecutive passes with interrogation windows of sizes 83×83, 62×62, 41×41 and 21×21 µm; and finalized with a sub-pixel pass in Fourier-space. Only the speeds measured inside the previously detected vessel segments were retained and projected onto the tangent of the segment. The orientation of each segment was then adjusted based on the maximal correlation between average speeds. Speeds from all aligned segments were then binned into a 2D histogram of resolution 350 ms × 6 µm/s, and the most likely hemolymph flow was computed using a shortest path approach , implemented using dynamic programming (. Finally, to dampen the effect of the binning required by dynamic programming, the resulting hemolymph flow was smoothed using cubic smoothing splines.

Ampullar contractions were measured as follows. We first identified ampullae in every frame as regions darker than 20× the estimated standard deviation of the image's white noise . The resulting binarized image was then consecutively morphologically opened and closed, using a structuring disk of radius 9.5 µm. The area and the centroid of each separated object was computed, and the trajectory of each ampulla was reconstructed by clustering across frames detections whose centroids were closer than 19 µm. Only trajectories that spanned more than 95 % of the frames were kept for further analysis. All the code written for our analysis was implemented as a set of custom MATLAB R2015b (MathWorks) functions and is available upon request.

Results

Hemolymph circulation

As a first step towards dissecting WBR, we characterized the hematological properties of a healthy and intact adult colony of *B. leachii* (Fig. 1 A-B). Hemolymph circulation in suspension-feeding ascidians undergoes a periodic reversal of flow direction between advisceral (towards the viscera) and abvisceral (towards the branchial basket). The advisceral flow starts on the anterior side of the heart, moves towards the endostyle before arriving to the pharynx and the mid-dorsal vessel, which supplies hemolymph to the digestive tract, and lastly passes to the dorsal end of the heart .

Utilizing the transparency of the tunic, we recorded time-lapse stereomicroscopy data from eight colonies at different locations in their vascular system (Fig. 1 C-F, Movies 1). Focusing on the largest vessels of the colony (Movie 1-2), we gathered a set of reproducible flow measurements (n=9, from 5 different colonies) that allowed us to calculate, using a custom-made PIV-based tracking software, the flow (peak velocity ~200µm/s) and reversal rates (~57/24 s) of a *B. leachii* colony (Fig. 2 A-C).

When recording vascular junctions, we observed (Movie 1) and quantified (Movie 3) an apparently pseudo-erratic pattern at the time of flow reversal. By examining terminal vessels (Movie 1), we extracted valuable information on the rate (11.4 ± 5.3 $\mu m^2/s$, n=18) and extent (dilated/contracted surface ratio: 1.55 ± 0.26, n=12) of the ampullar contraction-dilatation cycle concomitant with hemolymph flow in ascidians . While the general timing of hemolymph and ampullae alternation is synchronized (average lag: 2.9 ± 2.5 s, n=24), small variations on the exact time of contraction for each ampulla could be measured (± 3.1 s, n=24, Fig. 2 D-F).

Hemocyte classification

By combining previous classification schemes for botryllid ascidians , we propose a generalized classification of *B. leachii* circulatory hemocytes into five functional groups: undifferentiated cells, immunocytes, mast cell-like cells, transport cells and storage cells (Table 1). A further detailed description of the observed cell types is provided in Table S1. In this classification, undifferentiated cells are composed solely of hemoblasts, also called lymphocytes or lymphocyte-like cells. Immunocytes can be further classified between phagocytes and cytotoxic cells. Phagocytes include hyaline amebocytes and macrophage-like cells while cytotoxic cells include granular amebocytes and morula cells. Mast-like cells are represented only by granular cells. Transport cells are composed of compartment amebocytes and compartment cells. Finally, storage cells include both pigment cells and nephrocytes. A comprehensive guide to hemocyte identification using bright field Giemsa stained images is provided (Table 2), with high magnification pictures exemplifying the most common aspect of each cell type (Fig. 3).

Altogether, these descriptions (Table 2) and images (Fig. 3) allowed us to identify most of the cells both in hemolymph smears and histological sections and provide an unambiguous identification reference for the analysis of the localization and fate of *B. leachii hemocytes* in the colony.

Asexual budding

To obtain a precise picture of the prevailing mode of asexual reproduction, we revised various stages of blastogenesis in *B. leachii* previously described by using histological sections. Palleal reproduction involves the formation of a new bud from the peribranchial epithelium of a zooid. Remarkably, in *B. leachii* blastogenesis starts very early in the development of a maturing bud, there are typically three generations co-existing in the colony (Fig. 4 A): second-generation buds (budlets), developing from more differentiated buds (first-generation buds), themselves attached to adult filter-feeding zooids (blastozooids).

The first visible sign of blastogenesis is the appearance of a bud disc, a thickened disk of cells on the ventral side of the atrial epithelium of a first-generation bud, just before the stage where its stigmata become perforated. In healthy colonies, one bud disc usually appears on each side of the forming pharyngeal basket (Fig. 4 B), thus producing two budlets and increasing the overall size of the colony. In well-fed colonies, one of these buds can even divide to give rise to two buds on one side of the zooid, producing one further zooid . The disc cells then proliferate until the bud reaches around 12 cells of diameter (day 1 of the second-generation development), protrudes outside of the first-generation bud through its mantle into the tunic (Fig. 4 C) and curves to form a hollow sphere of cells inside a mantle pouch highly reminiscent of the early stages of blastogenesis (days 2-3). This pouch connects the growing bud with the hemocoel of the mother bud, ensuring that hemolymph and oxygen reach the new bud while the rudiment for the vascular connection to the rest of the colony will be initiated underneath by an outgrowth of the epithelium layer , later producing the radial vessel .

The asexually developing bud continues to increase in size and begins to fold, forming three main compartments, which will form the internal structures of the new adult (days 4-6, Fig. 4 D). It is at that stage that the first signs of germ cells can also be observed (Fig. 4 D). The folds will ultimately join, creating the basic structure for the pharyngeal basket (days 7-8). Once the extending pharyngeal basket has joined the stomach and started to produce its first stigmata, the stereotypical body plan of the zooid is completed, thus becoming a first-generation bud on which new budlets start to appear (day 9, Fig. 4 E). Following this stage, the first-generation bud will differentiate into a fully

functional zooid hence growing in size, finalizing its various organs and vascular system (days 10-22, Fig. 4 F), starting its cardiac activity around day 17.

In total, it takes approximately 22 days at 17 °C to produce a functioning zooid through blastogenesis . Afterwards, the zooid will feed for another 8 days before it gets resorbed through a whole-body apoptosis (< 3 days), in which numerous large macrophage-like cells infiltrate and remove effete cells from the senescent tissues (Franchi *et al.*, 2016) and the next generation succeeds.

***B. leachii* whole-body regeneration**

The vascular and hematological characteristics of WBR in *B. leachii*, are described through comparisons with blastogenesis and intact colonies (Fig. 5). For this analysis, we follow a published classification of WBR into 5 stages (Fig. 1 G; : Stage 0, injury of the colony; Stage 1, healing of the injury; Stage 2, remodeling of the vascular system; Stage 3, condensation of the ampullae; Stage 4, establishment and development of regeneration niches; Stage 5, fully regenerated zooid.

Stage 0: Injury (0 h)

B. leachii has a great capacity for preventing hemolymph loss from injuries, with hemolymph loss stopped in less than 30 s by a combination of tissue contraction and hemocyte aggregation (Movie 4). Upon ablation of the zooids, the remaining vascular tissue initially looses a small volume of hemolymph but quickly contracts its peripheral vessels to halt the oozing and hemocytes starts to aggregate (Fig. 5 A). Flow will then restart after a pause, the duration of which is seemingly related to either the number of ampullae or the amount of vascular tissue, but was consistently shorter than 10 min. We observed restart of hemolymph flow in as little as two minutes (Movie 4), starting in the portion of the tissue furthest away from the injury in an erratic yet bidirectional fashion, and progressively re-spanning almost the entire vascular system (Movie 4). Although driven only by ampullar contractions, this novel hemolymph flow exhibits a reversal frequency similar to that of intact vessels in a whole colony. As suspected, given the short amount of time available for new cellular differentiation, the composition of this hemolymph is almost identical to the one from intact colonies, with a slight increase in the population of granular cells (Fig. 5 G).

Stage 1: Wound healing (15 h)

At this stage of WBR, a dramatic amount of extravascular cellular activity is taking place. The two most apparent aspects are the infiltration of morula cells into the tunic and the remodeling of the tunic matrix (Fig. 5 B). When focusing on circulating hemocytes, we observed an incipient decrease in the population of morula cells, accompanied with an increase in the populations of hemoblasts, hyaline amebocytes, and granular cells (Fig. 5 G).

Stage 2: Ampulla remodeling (24 h)

Concomitant with the observed wound healing process, terminal ampullae start changing their elongated shape to a more spheroid form, contracting, and creating novel tunic vessels (Fig. 5 C; . One day after injury, previously reported giant cells could be observed throughout the vascular system (Fig. 5 C). In addition, this step exhibits the first signs of the subsequent increase in phagocytic cells (Fig. 5 G).

Stage 3: Tissue contraction (2 – 4 d)

By stage 3, the vascular system had fully contracted into a dense network and various regeneration niches were visible within the tissue (Fig. 5 D). Regeneration niches are defined as spherical aggregates of cells within the vascular lumen. Probably the most striking change, at this stage of WBR, was the large increase in phagocytic cells (Fig. 5 D & G), while numbers of both hemoblasts and differentiating cells had returned to pre-injury levels (Fig. 5 G).

Stage 4: Regeneration niches (5 – 7 d)

During stage 4, several regeneration niches were present and the foundation of an adult could be observed within one of them (Fig. 5 E). Nonetheless, only one zooid will regenerate and the less developed niches will be resorbed . Advanced niches already displayed well developed axial and tissue organizations reminiscent of the early first-generation stage of blastogenesis (Fig. 4 E), including an endostyle as well as an imperforated pharyngeal basket (Fig. 5 E). In comparison to palleal budding, the regenerating buds were lacking visible gametes (compare Fig. 4 E and Fig. 5 E).

At this stage of WBR, hemolymph flow can be observed in novel tunic vessels (Movie S5), and the composition of the hemolymph strives towards the composition observed in intact colonies. Transport, mast-cell like, and storage cells are at their lowest during this period while hyaline amebocytes and macrophage-like cells remain at a higher proportion than in uninjured colonies (Fig. 5 G).

Stage 5: Regenerated zooid (8 – 10 d)

At the conclusion of WBR, a single fully functional zooid is regenerated, displaying the palleal buds expected from an uninjured adult (Fig. 5 F). The hemolymph composition of this new adult is largely similar to that of an intact colony, albeit with a slightly smaller phagocytic cell population (Fig. 5 G).

Discussion

Here, we carefully dissected the hematological and histological properties of both intact and regenerating *B. leachii* colonies. We compared hemolymph flow patterns to published data from related ascidian species and revised previous studies on *B. leachii* asexual development. In addition, we followed the quantity and location of each type of hemocyte during whole-body regeneration, finding that regeneration progresses through a rapid healing response, an increased activity of hemoblasts, the recruitment of macrophage-like cells and finally their clearing from the hemolymph.

Synchronization of blood flow in intact and regenerating colonies

Using time-lapse recording, we were able to quantify the complex hemolymph flow patterns observed within a *B. leachii* colony. While the velocity of hemolymph in ascidians has to our knowledge not yet been estimated, the measured average velocity predicts that hemocytes travel an average of 8 mm during one alternation of the flow. In such a small organism (~2 mm in length), this range could be critical for spreading signaling metabolites and thus potentially coordinating colony responses. The values we obtained for the reversal rates are similar to those measured in other ascidian species, albeit slightly more asymmetric and with a relatively shorter advisceral period (21 to 36 s in *B. leachii*, 30 to 50 s in *Botryllus primigenus* and 45 to 60 s in *Symplegma reptans*; . We also observed a quick reestablishment of a regular hemolymph flow after injury, and despite the removal of all zooids from the vascular system. This flow is thus sustained solely by synchronized and localized patterns of ampullar contractions (Fig. 2 G-I, Movie 4-5). While this synchronization could solely be a consequence of hemolymph pressure and elastic vascular tissue , the absence of any zooid heart within the tunic suggests the existence of a yet unidentified stimulus coordinating this activity.

Similar to vertebrates , *B. leachii* heart activity starts before the zooid is fully mature, when neither capable of filter feeding nor of using most of its other organs. Early heart function is consistent with the necessity to circulate oxygen and nutrients throughout the developing organism, even though the parental heart is connected directly to the hemocoel of the bud and would appear to be sufficient for sustaining such circulation. In fact, the pressure exerted by the parental heart is strong enough to impose its direction and reversal rate onto the daughters' heart .

Hemolymph composition in Styelidae

We have reported a detailed characterization of hemocytes in *B. leachii*. The identified cell types are compatible with previous reports in this species (Cima *et al.*, 2002), comparable to those in other ascidians (Cima *et al.*, 2014) and in particular to those of the same family (Styelidae; Ballarin and Kawamura, 2009; de Barros *et al.*, 2009; Gutierrez and Brown, 2017). Notably, while granular cells appear to be absent from other botryllid species (Hirose *et al.*, 2003; Ballarin *et al.*, 2011), they have been identified in *Styela plicata* (de Barros *et al.*, 2009), *Symplegma brakenhiemli* (Gutierrez and Brown, 2017) and even in *Thalia democratica* (Cima *et al.*, 2014). Their presence in more distant species of ascidians suggests either a loss in botryllids that did not affect *B. leachii* or that their visual characteristics are not observable in these botryllids. Further analyses with different staining techniques (Gutierrez and Brown, 2017) could help resolve this issue.

In addition, we here provide a quantification of the composition of hemolymph throughout WBR, which are particularly interesting to compare with those made in other Styelidae (Gutierrez and Brown, 2017). First, Morula cells and Macrophage-like cells consistently compose the majority of hemocytes in this whole family of ascidians, highlighting the importance of the immune system in these organisms. Second, the amount of differentiating cells observed in *S. brakenhiemli* (19 %), a shorter-lived colonial species that undergoes continuous and asynchronous takeover, corresponds to the levels measured during stage 1 of WBR and emphasizes the strong requirement for tissue generation at this early stage. Third, the fraction of hyalin amebocyte is the lowest amongst all quantified Styelidae, potentially owing to a faster differentiation into macrophage-like cells. In addition, these hyalin amebocytes could be preferentially present outside of the hemocoel and thus be underrepresented in our counting. Finally, the extreme peak of macrophage-like cells measured during stage 3 is much greater than what is observed during the normal life-cycle of Styelidae. One potential explanation is that, during takeover, the period when the colony is unable to feed is much shorter, or even totally absent in *S. brakenhiemli*, thus there could be a lesser need for storage of nutrients by these cells.

Morphological and cellular changes during distinct phases of *B. leachii* WBR

We additionally characterized the morphological and hematological modulation of injured colonies throughout WBR. Morula cells are known constituents of the immune system involved in inflammatory responses, hemolymph aggregation, homeostasis, and tunic repair . The large number of infiltrated morula cells observed during stage 1 of WBR highlights a need for both clearance of decaying or foreign debris and reorganization of the injured vascular system during the first 15 h post dissection. In addition, we measured an increase in the population of differentiating cells (Fig. 5 G), consistent with the need to re-establish homeostasis within the *B. leachii* vasculature and to compensate for hemolymph loss. An increased number of mast cell-like cells, a cell type apparently absent from related ascidian species , was also observed. While their role remains unclear, two hypothesis have been proposed: either a source of

nourishment or the immunosurveillance of the alimentary tract . Their presence during WBR, in the absence of any feeding zooid, rather supports a nutritive role.

At stage 2, we observed the first signs of the subsequent increase in phagocytic cells, potentially as a result of the previously observed differentiation activity (Fig. 5 G) and of the inflammatory response induced by the morula cells (Fig. 5 B). Given the role of these macrophage-like cells in the removal of foreign elements from the tissue , their presence during stage 3 of WBR points towards a recruitment for undertaking the clearing of bacteria, dead cells, and residues of remodeled tunic. The concomitant reduction of hemoblasts to pre-injury levels suggests that the wound healing and remodeling phase has been completed, and that cellular proliferation as well as differentiation have returned to hemopoietic levels within the vascular system. Finally, during stage 4, mast cell-like, transport, and storage cells were observed at their lowest level throughout WBR. This could be a direct consequence of the imposed absence of feeding, leading to a lack of nutrients to be transported or stored. Regenerating *B. leachii* colonies would then need to obtain nutrients in an alternative way. Similar to reactivation of hibernating colonies and to the takeover of a new generation of buds in *B. schlosseri* , extraction of reserve nutrients from macrophage-like cells would supplement this need and gradually reduce the number of phagocytic cells, as observed experimentally (Fig. 5 G).

When focusing on vascular circulation, the initial rapid interruption in hemolymph flow (Movie 4) could be a consequence of either the reduced density of hemolymph inside the vascular system, or an actively regulated mechanism to reduce the pressure at the sectioned vessels and aiding aggregation. Given that hemolymph flow restarts over a relatively short time scale compared to that necessary for substantial hemocytes production and pressure increase, the latter hypothesis appears more likely. This observation thus further supports the existence of an unidentified stimulus systemic to the entire vascular system, potentially relayed directly by the epithelial cells lining the vasculature .

Similarities and divergences between blastogenesis and WBR

The major discrepancy between blastogenesis and WBR was the absence during WBR of visible gametes (Fig. 5 E). As WBR restores both the soma and the germ line , the absence of gametes in regenerating niches indicates that they will be created during subsequent cycles of blastogenesis. This process may be an energetically economical developmental approach that avoids the production of gametes in niches that could subsequently be resorbed. Overall, once the vascular tissue has fully contracted, the timing of WBR initially relates closely to that of blastogenesis (day 1-8), but ultimately produces a functional adult much faster. One potential cause for such increased speed is the temperature at which the regenerating colonies were kept (~19 °C in the present study), which is known to directly correlate with developmental pace . Temperature alone may not entirely explain such difference in timing however, and one likely cause could be that functional regenerated zooids are smaller than palleal ones, thus having a shortened growth phase which normally spans more than half of blastogenesis. Indeed, such reduction in zooid size was observed in *B. schlosseri* .

Conclusion

Overall, this study underlines the complex interplay of mechanisms required for successful WBR, and complements previous morphological studies by providing a higher temporal resolution. Our histological analysis of WBR supports our recent sequencing approach that identified an initial healing phase followed by a regeneration response and have provided the first detailed account of the hematological properties of *Botrylloides leachii* colonies throughout whole-body regeneration.

Acknowledgements

We would like to thank Francesca Cima (Department of Biology, University of Padova) for pieces of advice, protocols and general help on hemocytes, as well as for proofreading this article; Rueben Pooley (Department of Marine Science, University of Otago) for his help in animal husbandry; Lorryn Fisher (Department of Anatomy, University of Otago) for providing the PCNA antibody; Noel Jhinku (Department of Pathology, University of Otago) for providing the rotifers; Kendall Gadomski (Department of Marine Science, University of Otago) for providing the All-G-Rich powder; Kristian Sveen (Institute for Energy Technology, University of Oslo) for developing the original code of MatPIV; Cynthia A. Brewer (GeoVISTA Center, Pennsylvania State University) for developing ColorBrewer; Fernando Romero Balestra (Department of Cell Signaling, CABIMER), Aude Blanchoud and Anna Jaźwińska (Department of Biology, University of Fribourg), for proofreading this article.

M.W. was funded by a Dean's Bequest Grant and by the Department of Anatomy [Otago University]; S.B. by the Swiss National Science Foundation (SNSF) [grant number P2ELP3_158873]; and L.Z. by a University of Otago Post-graduate scholarship.

Literature cited

Ballarin, L., A. Franchini, E. Ottaviani and A. Sabbadin. **2001**. Morula cells as the major immunomodulatory hemocytes in ascidians: Evidences from the colonial species *Botryllus schlosseri*. *Biol. Bull.* **201**: 59–64.

Ballarin, L. and F. Cima. **2005**. Cytochemical properties of *Botryllus schlosseri* hemocytes: indications for morpho-functional characterization. *Eur. J. Histochem.* **49**: 255–64.

Ballarin, L. and K. Kawamura. **2009**. The hemocytes of *Polyandrocarpa misakiensis* : morphology and immune-related activities. *Invertebr. Surviv. J.* **6**: 154–161.

Ballarin, L., M. del Favero and L. Manni. **2011**. Relationships among hemocytes, tunic cells, germ cells, and accessory cells in the colonial ascidian *Botryllus schlosseri*. *J. Exp. Zool. Part B Mol. Dev. Evol.* **316B**: 284–295.

Bellman, R. 1952. On the theory of dynamic programming. *Proc. Natl. Acad. Sci. U. S. A.* **38**: 716–9.

Berrill, N. J. 1941. The development of the bud in *Botryllus*. *Biol. Bull.* **80**: 169.

Berrill, N. J. 1947. The developmental cycle of *Botrylloides*. *Q. J. Microsc. Sci.* **88**: 393–407.

Brewin, B. I. 1946. Ascidians in the vicinity of the Portobello Marine Biological Station, Otago Harbour. *Trans. R. Soc. New Zeal.* **76**: 87–131. Transactions and Proceedings of the Royal Society of New Zealand 1868-1961.

Brown, F. D., E. L. Keeling, A. D. Le and B. J. Swalla. **2009**. Whole body regeneration in a colonial ascidian, *Botrylloides violaceus*. *J. Exp. Zool. B. Mol. Dev. Evol.* **312**: 885–900.

Brown, F. D. and B. J. Swalla. **2012**. Evolution and development of budding by stem cells: Ascidian coloniality as a case study. *Dev. Biol.* **369**: 151–162. Elsevier.

Brunetti, R. 1976. Biological cycle of *Botrylloides leachi* (Savigny) (Ascidiacea) in the Venetian lagoon. *Vie Milieu* **XXVI**: 105–122.

Brunetti, R. 2009. Botryllid species (Tunicata, Ascidiacea) from the Mediterranean coast of Israel, with some considerations on the systematics of Botryllinae. *Zootaxa* **2289**: 18–32.

Burighel, P. and R. Brunetti. **1971**. The circulatory system in the blastozooid of the colonial ascidian Botryllus Schlosseri (Pallas). *Bolletino di Zool.* **38**: 273–289.

Burighel, P., R. Brunetti and G. Zaniolo. **1976**. Hibernation of the colonial ascidian *Botrylloides leachi* (Savigny): histological observations. *Ital. J. Zool.* **43**: 293–301.

Cima, F. 2010. Microscopy methods for morpho-functional characterisation of marine invertebrate haemocytes. *Microsc. Sci. Technol. Appl. Educ.* 1100–1107.

Cima, F., A. Perin, P. Burighel and L. Ballarin. **2002**. Morpho-functional characterization of haemocytes of the compound ascidian *Botrylloides leachi* (Tunicata, Ascidiacea). *Acta Zool.* **82**: 261–274.

Cima, F., F. Caicci and P. Sordino. **2014**. The haemocytes of the salp *Thalia democratica* (Tunicata, Thaliacea): An ultrastructural and histochemical study in the oozoid. *Acta Zool.* **95**: 375–391.

de Barros, C. M., D. R. de Carvalho, L. R. Andrade, M. S. G. Pavão and S. Allodi. **2009**. Nitric oxide production by hemocytes of the ascidian *Styela plicata*. *Cell Tissue Res.* **338**: 117–128.

de Leo, G. 1992. Ascidian hemocytes and their involvement in defence reactions. *Bolletino di Zool.* **59**: 195–214.

Delsuc, F., H. Brinkmann, D. Chourrout and H. Philippe. **2006**. Tunicates and not cephalochordates are the closest living relatives of vertebrates. *Nature* **439**: 965–968.

Dijkstra, E. W. 1959. A note on two problems in connexion with graphs. *Numer. Math.* **1**: 269–271.

Dijkstra, J., A. Dutton, E. Westerman and L. G. Harris. **2008**. Heart rate reflects osmostic stress levels in two introduced colonial ascidians *Botryllus schlosseri* and *Botrylloides violaceus*. *Mar. Biol.* **154**: 805–811.

Endean, R. 1960. The blood-cells of the ascidian, Phallusia Mammillata. *J. Cell Sci.* **s3-101**: 177–197.

Ermak, T. H. 1982. The renewing cell populations of ascidians. *Am. Zool.* **22**: 795–805.

Franchi, N., F. Ballin, L. Manni, F. Schiavon, G. Basso and L. Ballarin. **2016**. Recurrent phagocytosis-induced apoptosis in the cyclical generation change of the compound ascidian *Botryllus schlosseri*. *Dev. Comp. Immunol.* **62**: 8–16. Elsevier Ltd.

Freeman, G. 1964. The role of blood cells in the process of asexual reproduction in the tunicate *Perophora viridis*. *J. Exp. Zool.* **156**: 157–183.

Goodbody, I. 1975. The physiology of ascidians. *Adv. Mar. Biol.* **12**: 1–149.

Gross, L. 2007. From one to many and back again: a systemic signal triggers tunicate regeneration. *PLoS Biol.* **5**: e98.

Gutierrez, S. and F. D. Brown. **2017**. Vascular budding in *Symplegma brakenhielmi* and the evolution of coloniality in styelid ascidians. *Dev. Biol.* **423**: 152–169. Elsevier Inc.

Hirose, E., M. Shirae and Y. Saito. **2003**. Ultrastructures and classification of circulating hemocytes in 9 botryllid ascidians (chordata: ascidiacea). *Zoolog. Sci.* **20**: 647–656.

Jaźwińska, A. and P. Sallin. **2016**. Regeneration versus scarring in vertebrate appendages and heart. *J. Pathol.* **238**: 233–246.

Lauzon, R. J., C. Brown, L. Kerr and S. Tiozzo. **2013**. Phagocyte dynamics in a highly regenerative urochordate: insights into development and host defense. *Dev. Biol.* **374**: 357–73. Elsevier.

Lauzon, R. J., K. J. Ishizuka and I. L. Weissman. **2002**. Cyclical generation and degeneration of organs in a colonial urochordate involves crosstalk between old and new: A model for development and regeneration. *Dev. Biol.* **249**: 333–348.
Liao, Q. and E. A. Cowen. **2005**. An efficient anti-aliasing spectral continuous window shifting technique for PIV. *Exp. Fluids* **38**: 197–208.
Menin, A., M. Del Favero, F. Cima and L. Ballarin. **2005**. Release of phagocytosis-stimulating factor(s) by morula cells in a colonial ascidian. *Mar. Biol.* **148**: 225–230.
Michaelsen, W. 1921. Die Botrylliden und Didemniden der Nordsee und der zur Ostsee fuhrenden Meeresgebiete. *Wissenschaftliche Meeresuntersuchungen (Abteilung Helgoland)* **14**: 99–124.
Milkman, R. 1967. Genetic and developmental studies on *Botryllus schlosseri*. *Biol. Bull.* **132**: 229.
Millar, D. A. and N. A. Ratcliffe. **1989**. The evolution of blood cells: facts and enigmas. *Endeavour* **13**: 72–7.
Miquerol, L. and R. G. Kelly. **2013**. Organogenesis of the vertebrate heart. *Wiley Interdiscip. Rev. Dev. Biol.* **2**: 17–29.
Mukai, H., Y. Saito and H. Watanabe. **1987**. Viviparous development in *Botrylloides* (compound ascidians). *J. Morphol.* **193**: 263–276.
Mukai, H., K. Sugimoto and Y. Taneda. **1978**. Comparative studies on the circulatory system of the compound ascidians, *Botryllus*, *Botrylloides* and *Symplegma*. *J. Morphol.* **157**: 49–78.
Oka, H. and H. Watanabe. **1957**. Vascular budding, a new type of budding in *Botryllus*. *Biol. Bull.* **112**: 225.
Oka, H. and H. Watanabe. **1959**. Vascular budding in *Botrylloides*. *Biol. Bull.* **117**: 340.
Paul, P., H. Duessmann, T. Bernas, H. Huber and D. Kalamatianos. **2010**. Automatic noise quantification for confocal fluorescence microscopy images. *Comput. Med. Imaging Graph.* **34**: 426–434.
Rinkevich, B., Z. Shlemberg and L. Fishelson. **1995**. Whole-body protochordate regeneration from totipotent blood cells. *Proc. Natl. Acad. Sci. U. S. A.* **92**: 7695–9.
Rinkevich, Y., G. Paz, B. Rinkevich and R. Reshef. **2007**. Systemic bud induction and retinoic acid signaling underlie whole body regeneration in the urochordate *Botrylloides leachi*. *PLoS Biol.* **5**: e71.
Rinkevich, Y., B. Rinkevich and R. Reshef. **2008**. Cell signaling and transcription factor genes expressed during whole body regeneration in a colonial chordate. *BMC Dev. Biol.* **8**: 100.
Rinkevich, Y., A. Rosner, C. Rabinowitz, Z. Lapidot, E. Moiseeva and B. Rinkevich. **2010**. *Piwi* positive cells that line the vasculature epithelium, underlie whole body regeneration in a basal chordate. *Dev. Biol.* **345**: 94–104. Elsevier Inc.
Sabbadin, A. 1969. The compound ascidian *Botryllus schlosseri* in the field and in the laboratory. *Pubbl Staz Zool Napoli* **37**: 62–72.
Sánchez Alvarado, A. and P. A. Tsonis. **2006**. Bridging the regeneration gap: genetic insights from diverse animal models. *Nat. Rev. Genet.* **7**: 873–884.
Savigny, J.-C. 1816. *Mémoires sur les animaux sans vertèbres*. Dufour, G., Paris.
Seifert, A. W., S. G. Kiama, M. G. Seifert, J. R. Goheen, T. M. Palmer and M. Maden. **2012**. Skin shedding and tissue regeneration in African spiny mice (*Acomys*). *Nature* **489**: 561–5. Nature Publishing Group.
Tanaka, E. M. and P. W. Reddien. **2011**. The cellular basis for animal regeneration. *Dev. Cell* **21**: 172–185. Elsevier Inc.
Voskoboynik, A., N. Simon-Blecher, Y. Soen, B. Rinkevich, A. W. De Tomaso, K. J. Ishizuka and I. L. Weissman. **2007**. Striving for normality: whole body regeneration through a series of abnormal generations. *FASEB J.* **21**: 1335–44.
Voskoboynik, A., Y. Soen, Y. Rinkevich, A. Rosner, H. Ueno, R. Reshef, K. J. Ishizuka, K. J. Palmeri, E. Moiseeva, B. Rinkevich, *et al.* 2008. Identification of the endostyle as a stem cell niche in a colonial chordate. *Cell Stem Cell* **3**: 456–64.
Wright, R. K. 1981. Urochordates. In: *Invertebrate blood cells. Volume 2. Arthropods to urochordates, invertebrates and vertebrates compared* (N. A. Ratcliffe and A. F. Rowley, eds), pp. 565–626. Academic Press, London.
Wright, R. K. and T. H. Ermak. **1982**. Cellular defense systems of the protochordata. In: *Phylogeny and Ontogeny*, pp. 283–320. Springer US, Boston, MA.
Zaniolo, G., A. Sabbadin and C. Resola. **1976**. Dynamics of the colonial cycle in the ascidian, *Botryllus schlosseri*. The fate of isolated buds. *Acta Embryol Exp* 205–213.
Zondag, L. E., K. Rutherford, N. J. Gemmell and M. J. Wilson. **2016**. Uncovering the pathways underlying whole body regeneration in a chordate model, *Botrylloides leachi* using de novo transcriptome analysis. *BMC Genomics* **17**: 114. BMC Genomics.

Tables

Table 1. Summary of cell types present in the *Botrylloides leachii* circulatory system.

Cell type	Subtype	Circulatory cells	Older terminology
Undifferentiated cell [c, d]	Hemoblast [e, f]	Hemoblast [e, f] Differentiating cell	Lymphocyte [a, b] Stem cell [d]
Immunocyte [c]	Phagocyte [e]	Hyaline amebocyte [d, f] Macrophage-like cell [d, f]	Amebocytes with vacuole [a] Signet ring cell [a, b] Vacuolated cell [c] Leukocyte [c]
	Cytotoxic cell [f]	Granular amebocyte [b, d, f] Morula cell [b, d, e]	Cells with acidic vacuole [a] Green cell [b] Leukocyte [c] Vanadocyte [a]
Transport cell [e]	Granulocyte [e]	Compartment amebocyte [d] Compartment cell [a, b, d]	Vacuolated cell [c]
Mast cell-like cell [g]	Granular cell [d]	Granular cell [d]	(Unique to *B. leachii*, [d])
Storage cell [f]	Vacuolated cell [f]	Pigment cell [a, c, d, e] Nephrocyte [c, d, e]	Cell with reflecting disks [a] Orange cell [b]

[a] (Endean, 1960); [b] (Freeman, 1964); [c] (Wright & Ermak, 1982); [d] (Cima et al., 2002); [e] (Hirose et al., 2003); [f] (Ballarin et al., 2011); [g] (Cima *et al.*, 2014)

Table 2. Classification chart of Botrylloides *leachii* hemocytes based on light microscopy Giemsa stain. Only the most common traits are listed in this table, refer to Table S1 for full description of the cell types.

Cell type	Size (µm)	Shape	Stain	Characteristic
Hemoblast	5 – 8	Round	Blue cytoplasm with a dark-blue nucleus	High nucleus to cytoplasm ratio
Differentiating cell	8 – 12	Swollen, irregular	Light-blue nucleus and grey cytoplasm	Fibrous cytoplasm with a proportionally large nucleus
Hyaline amebocyte	6 – 9	Amebocyte: highly irregular, including a variety of pseudopodia	Dual purple-blue cytoplasm	Purple stained clear cytoplasmic vesicles
Macrophage-like cell	6 – 20	Mostly round with irregular content	Blue with vesicles of varying shades of yellow, brown, green and grey	Vesicles highly heterogeneous in size, shape and content
Granular amebocyte	6 – 10	Amebocyte	Scattered dark-green cytoplasmic vesicles	Sparser vesicles than granular cells
Morula cell	10 – 16	Circular containing a low number of large (~2 µm), pale yellow and round vacuoles	Orange-green cytoplasmic color in smears, red color around the vacuoles in histological sections	Most common cell type in *B. leachii* hemolymph
Granular cell	8 – 12	Circular with irregular edge	Dense dark-blue/green vesicles	High density of vesicles renders the cell black and opaque
Compartment amebocyte	7 – 10	Amebocyte with a berry-like shape	Blue with a dark-blue nucleus	Numerous clear protruding vesicles
Compartment cell	12 – 18	Similar to morula	Unstained-grey opaque vesicles	Large uniform vesicles
Pigment cell	10 – 16	Similar to morula	Filled with minute dark granules, related to the colony color	The content of the vesicle exhibits Brownian movement in living cells
Nephrocyte	10 – 16	Berry-like	Dark and speckled grey vesicles	An aggregate of dark grey vesicles

Figures

Figure 1

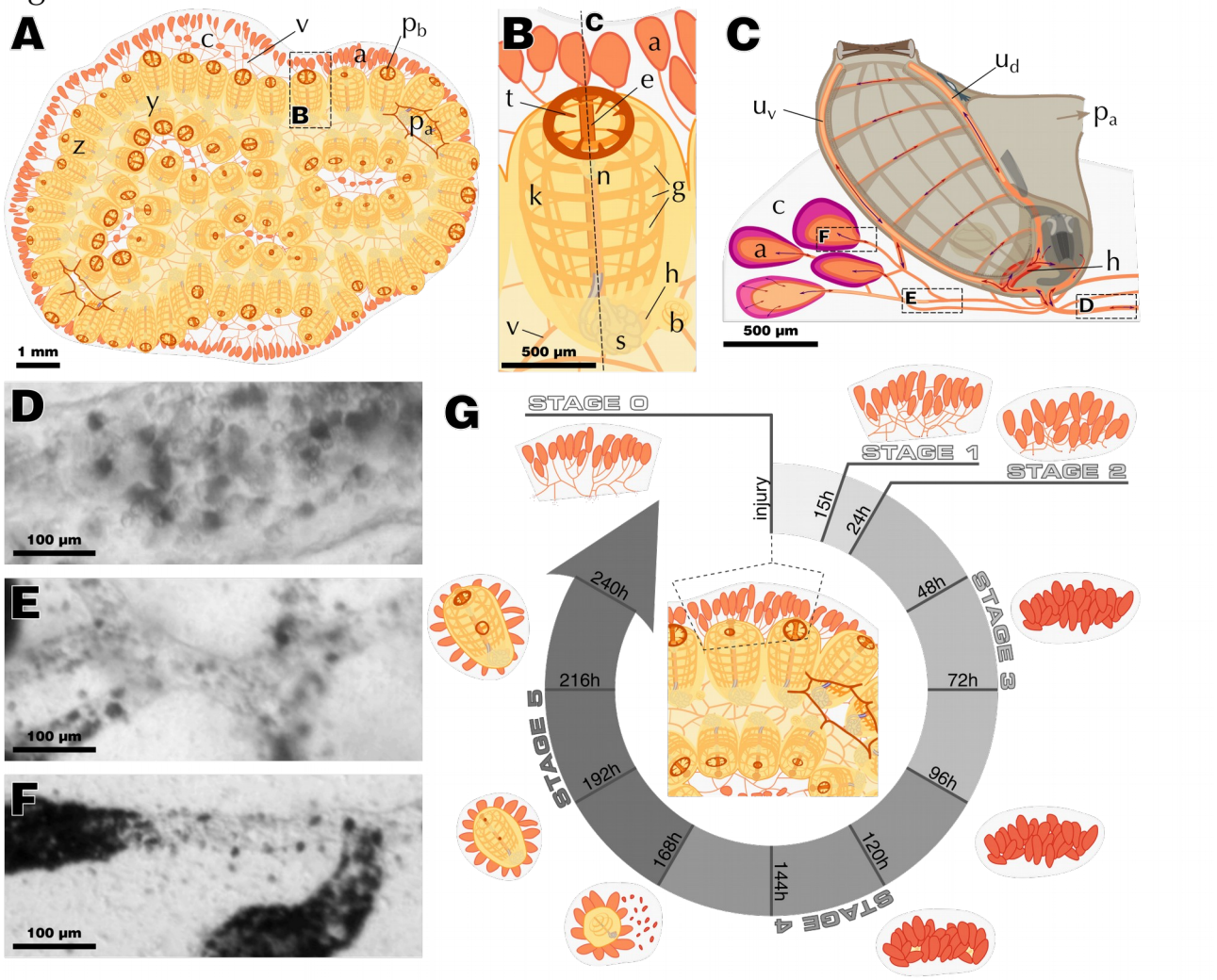

Fig. 1 ***Botrylloides leachii*** **schematic morphology and physiology.** Abbreviations: zooid (z), system (y), tunic (c), vascular system (v), terminal ampullae (a), buccal siphon (p_b), atrial siphon (p_a), oral tentacles (t), endostyle (e), pharyngeal basket (k), stigmata (g), neural ganglion (n), heart (h), stomach (s), bud (b), dorsal sinus (u_d), ventral sinus (u_v). (**A**) Top-view of a stereotypical colony composed of 72 zooids. Dashed-delimited area magnified in **B**. (**B**) Top-view of a single zooid. Longitudinal plane (dashed) depicted in **C**. (**C**) Left lateral view of a zooid. Abvisceral/advisceral hemolymph direction and contraction/dilatation of ampullae are depicted using the arrows. Dashed-delimited areas are exemplified in **D**-**F**. *In vivo* stereo-microscopic images of a large vessel (**D**), vascular junction (**E**) and terminal ampullae (**F**), taken from recordings showcased in Movie 1. (**G**) *B. leachii* WBR from a fragment of vascular tissue through our five defined stages and the approximate time-line

Figure 2

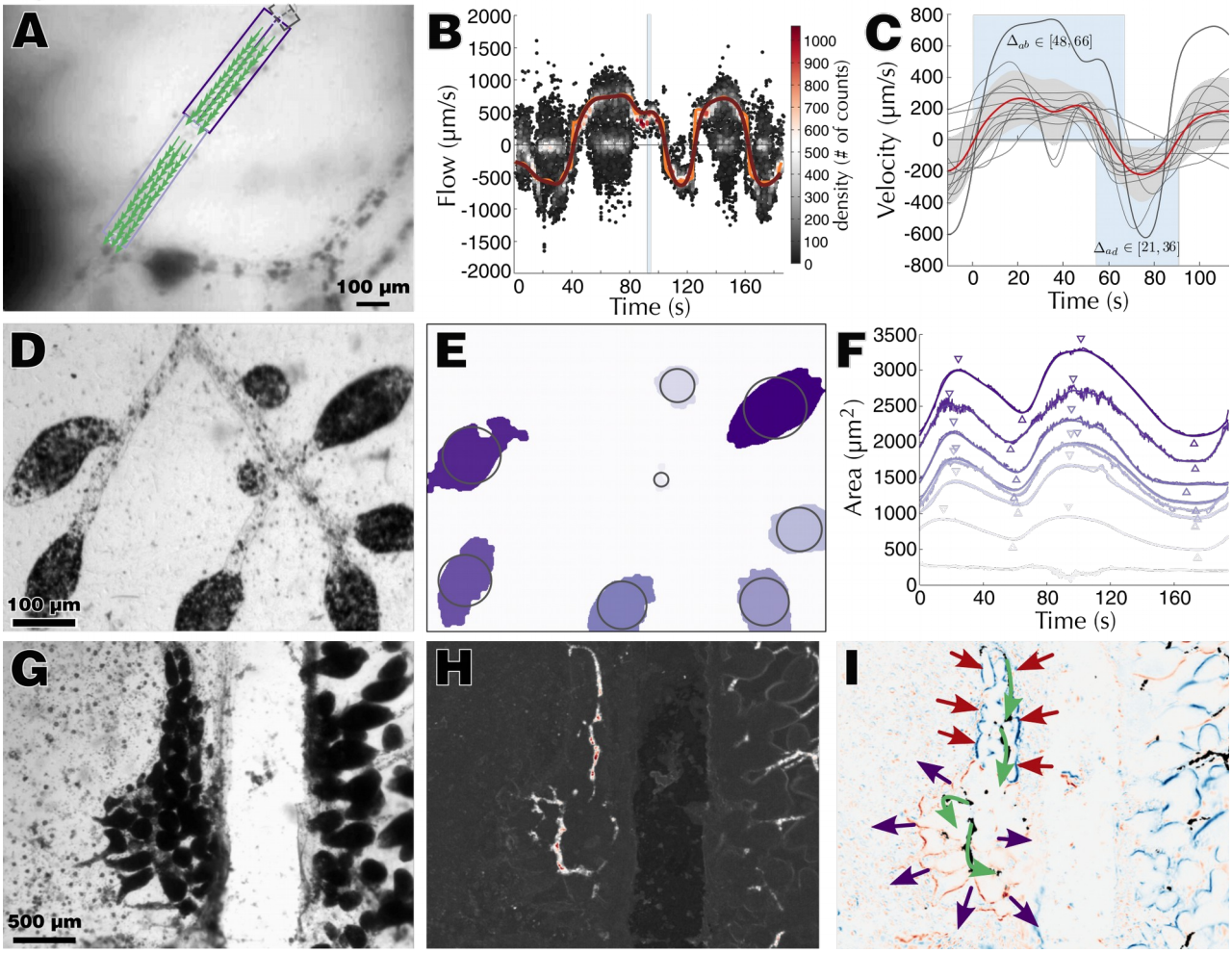

Fig. 2 Quantification of hemolymph circulation in *B. leachii*. (**A**) Raw frame overlaid with identified vessels (boxes) and PIV quantification (arrows). (**B**) 2D density histogram of PIV measurements (dots), inferred flow velocity (grey), smoothed velocity (light grey) and position of the frame displayed in **A** (dark grey rectangle). (**C**) Average (n=8) abvisceral hemolymph flow with individual recordings (thin grey lines), the recording utilized in **A**-**B** (thick grey line), the average velocity (black) and standard deviation (dark grey area). A visual representation of the abvisceral and advisceral phase durations is shown (light grey boxes). (**D**) Raw frame and (**E**) intensity-based detection of ampullae overlaid with centered circles of corresponding area. (**F**) Dilatation-contraction cycles of eight terminal ampullae from a single time-lapse recording. The raw data (darker line) is overlaid with a smoothed measurement (lighter line), local maxima and local minima (down and up triangles, respectively). The abvisceral phase of the hemolymph flow corresponds to the contraction phase of the ampullae. (**G**) Raw frame and (**H**) average absolute second order difference between frames depicting hemolymph flow (white). (**I**) Ampullae contractions are independent from heart activity and can drive hemolymph flow (grey arrows) by synchronized spatially restricted contractions (light grey arrows) and dilatations (dark grey arrows)

Figure 3

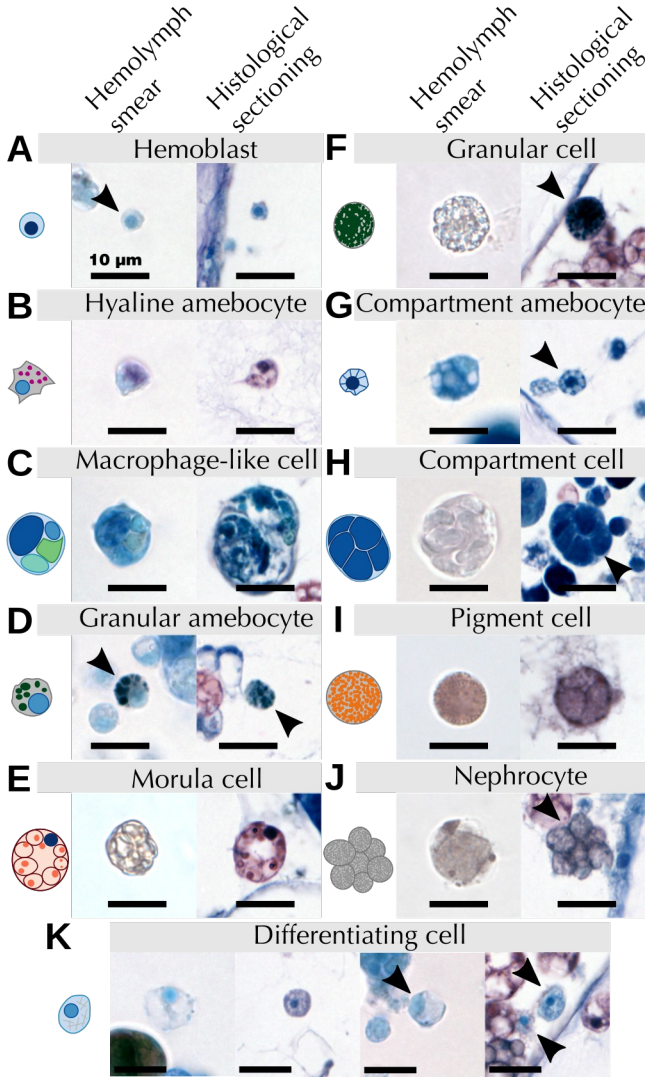

Fig. 3 Characterization of *B. leachii* hemocytes. Stereotypical schemas along with characteristic images of all hemocytes identified in *B. leachii* stained with Giemsa dye, both from hemolymph smears (left) and whole-colony histological sections (right). (**A**) hemoblasts, (**B**) hyaline amebocytes, (**C**) macrophage-like cells, (**D**) granular amebocytes, (**E**) morula cells, (**F**) granular cells, (**G**) compartment amebocytes, (**H**) compartment cells, (**I**) pigment cells, (**J**) nephrocytes and (**K**) undifferentiated cells. The illustrated cell is either located at the centre of the image or indicated by an arrowhead. Note that the cells in the histological sectioning show a degree of shrinkage following PFA fixation

Figure 4

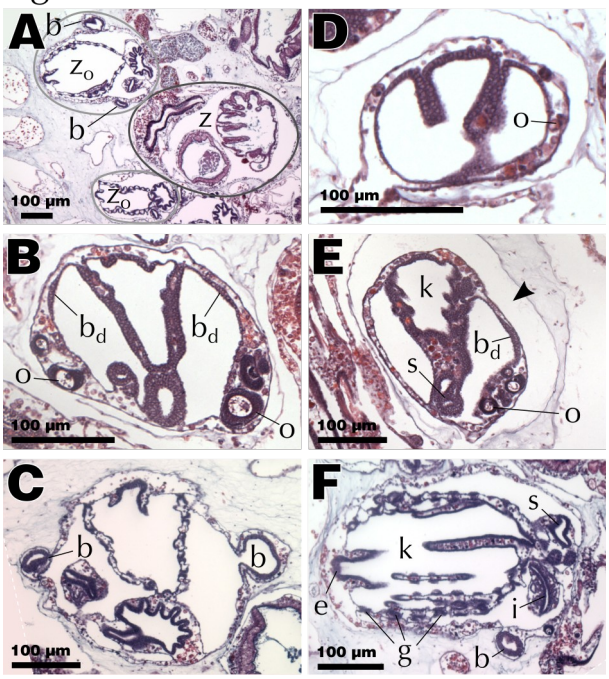

Fig. 4 Histology of palleal budding. Abbreviations: zooid (z), first-generation bud (z_o), second-generation bud (b), bud disc (b_d), oocyte (o), endostyle (e), pharyngeal basket (k), stigmata (g), intestine (i), stomach (s). All sections are stained with H&E. (**A**) Typical *B. leachii* asexual reproduction cycle with three generations co-existing: mature zooid (dark grey), two first-generation buds (light grey) and two budlets visible. (**B**) Bud developing two bud discs and oocytes. (**C**) First-generation bud with right budlet protruding and left budlet fully circular. (**D**) Young bud starting to invaginate. (**E**) Older bud with pharyngeal basket, tentative stigmata, a bud disc and oocytes. (**F**) Bud on the point of becoming a filter-feeding zooid

Figure 5

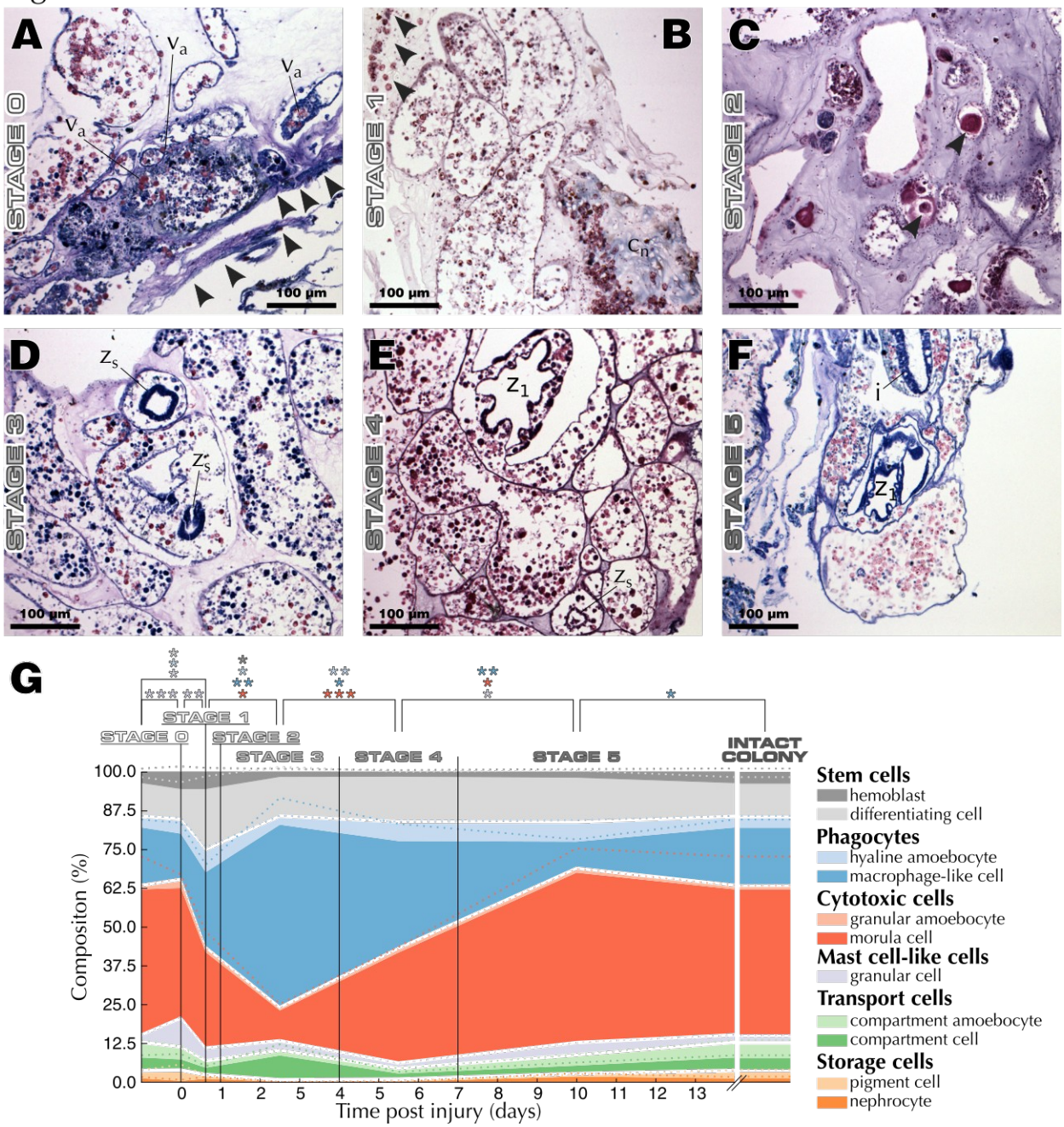

Fig. 5 Progression of *B. leachii* WBR. Abbreviation: hemolymph aggregate (v_a), collagen (c_n), spheroid bud (z_s), first-generation bud (z_o), intestine (i). (**A**) Stage 0: Giemsa stain of injured vascular tissue displaying signs of tunic contraction (arrowheads) and hemocyte aggregation. (**B**) Stage 1: Collagen remodeling and infiltration of cells into the tunic (arrowheads). Methyl blue within MSB dyes collagen blue. (**C**) Stage 2: H&E stained giant cells (arrowheads) throughout the remodeling vasculature. (**D**) Stage 3: Giemsa stained regeneration niches at different stages of development, and increase in macrophage-like cells (see **A** and **F**). (**E**) Stage 4: H&E stain shows competing regeneration niches at the first-generation and spheroid stages. (**F**) Stage 5: Giemsa stain of a fully regenerated zooid with first-generation bud. (**G**) Evolution of hemocyte types within ampullae throughout WBR, overlaid with the corresponding standard error (dotted lines) and stages of WBR (see Fig. 1G). Cell types are indicated in the legend. The color-coded asterisks show statistical significance between the corresponding populations (Student's two-tailed *t*-test, *: $P < 0.05$, **: $P < 0.01$, ***: $P < 0.001$)

Movie legends

Movie 1 Showcasing the various aspects of hemolymph flow in the vascular system of *B. leachii* vascular system using brightfield microscopy. Three different movies (from a large vessel, at a vascular junction and terminal ampullae, respectively) were combined to produce this presentation. The time and scale are specified on the frames of the recording in the top-left and bottom-right corners of the image, respectively. MPEG-4 recording file encoded with the H.264 codec

Movie 2 Hemolymph flow analyzed in Fig. 2 A-C. MPEG-4 recording file encoded with the H.264 codec

Movie 3 The turbulences of hemolymph flow at junctions during flow reversal. The upper panel depicts the measured hemolymph velocity in the various vessel segments, while the lower panel overlays the original recording with the detected vessel segments (blue) and hemolymph flow (red arrows). MPEG-4 recording file encoded with the H.264 codec

Movie 4 Time-lapse recording of injury-induced WBR. MPEG-4 recording file encoded with the H.264 codec

Movie 5 Time-lapse recording of WBR, 6 days post injury. The recorded tissue is the one visible in Movie 4. MPEG-4 recording file encoded with the H.264 codec

Table S1: Detailed description of hemolymph cell types present in the *B. leachii* vascular system based on histological observations.

Cell type (% of all hemocytes)	Description
Undifferentiated cells	
Hemoblast (4 %)	This small (5-8 µm), almost perfectly round, progenitor cell has a high nuclear-cytoplasmic ratio. It has a consistent dark blue nuclear stain, and most commonly a blue cytoplasmic stain. However, unstained or pink cytoplasmic staining was occasionally observed.
Differentiating cell (11 %)	A number of transitory cells can be identified in *B. leachii* hemolymph. Although it is difficult to determine which differentiation program these cells are following, the morphology of the majority of cells suggests that they originate from hemoblasts. These medium sized (8-12 µm) cells display a large light-blue stained nucleus, sometimes a nucleolus, and an unstained, often fibrous, grey cytoplasm with various morphological and staining features reminiscent of their future cell type.
Immunocytes	
Hyaline amebocyte (3 %)	As with all other amebocytes, this small (6-9 µm) cell has an irregular shape, typically displaying a large variety of pseudopodia. Hyaline amebocytes have a dual purple-blue cytoplasmic staining, where the purple appears to originate from a variety of clear vesicles. In histological sections, both entirely purple cells and purple cells with a blue crescent containing the nucleus were observed.
Macrophage-like cell (19 %)	This extremely variable cell (6-20 µm) shows a wide range of sizes and shapes depending on the material it engulfed. Therefore, although most of the cells were fully stained dark-blue, some colour variations (including shades of yellow, brown, green and grey) were observed depending on the ingested material. Empty macrophage-like cells display a red crested cytoplasm (Cima et al., 2002). Particularly in large cells, the nucleus is displaced towards the periphery of the cell by the phagocytic vacuoles. While they can resemble compartment cells, macrophage-like cells have a greater heterogeneity in the size, shape and content of their vesicles.
Granular amebocyte (1 %)	A small (6-10 µm) amebocyte characterized by a number of scattered dark-green cytoplasmic vesicles. While they resemble granular cells, granular amebocytes have a much lower density of granules, always displaying some portion of its cytoplasm. The cytoplasm is stained a light-blue/grey, although dark-blue and red have also been occasionally observed.
Morula cell (49 %)	This typically large (10-16 µm) cell is mostly characterized in smears by its orange-green cytoplasmic colour, and in histological sections by the red colour of the thin cytoplasm among the large vacuoles. It displays low numbers of large (~2 µm), pale yellow and round vacuoles, thus resulting in its characteristic berry-like shape.
Mast cell-like cells	
Granular cell (1 %)	A medium-sized (8-12 µm) cell, mostly circular, with a very irregular edge owing to the numerous small vesicles it contains. A variety of vesicles have been observed, but the majority are stained dark-blue/green and packed at such a high density that the whole cell appears black and opaque.
Transport cells	
Compartment amebocyte (5 %)	A small (7-10 µm) amebocyte characterized by numerous clear protruding vesicles, resulting in a berry-like shaped cell when observed unfixed. Its cytoplasm stains blue, with a dark blue nucleus easily visible in sections but harder to find in smears.
Compartment cell (4 %)	Large (12-18 µm) cell that displays few (typically less than 12) but large (~3 µm) opaque vesicles that remain mostly unstained-grey.
Storage cells	
Pigment cell (2 %)	A medium-sized (10-16 µm) cell that displays a number of large vacuoles filled with characteristic minute dark granules, whose colour relates to that of the colony (dark orange in this particular example).
Nephrocyte (1 %)	This medium-sized (10-16 µm) cell closely resembles pigment cells but lacks any pigment colour. These cells do not exhibit a circular shape filled with vesicles but rather a berry-like shape, as an aggregate of vesicles.